

D. Tskhakaya et al.

Kinetic Modelling of the Detached Divertor Plasma

15th International Workshop on Plasma Edge Theory in Fusion Devices
Nara, Japan
(9th September 2015 – 11th September 2015)

“This document is intended for publication in the open literature. It is made available on the clear understanding that it may not be further circulated and extracts or references may not be published prior to publication of the original when applicable, or without the consent of the Publications Officer, EUROfusion Programme Management Unit, Culham Science Centre, Abingdon, Oxon, OX14 3DB, UK or e-mail Publications.Officer@euro-fusion.org”.

“Enquiries about Copyright and reproduction should be addressed to the Publications Officer, EUROfusion Programme Management Unit, Culham Science Centre, Abingdon, Oxon, OX14 3DB, UK or e-mail Publications.Officer@euro-fusion.org”.

The contents of this preprint and all other EUROfusion Preprints, Reports and Conference Papers are available to view online free at <http://www.euro-fusionscipub.org>. This site has full search facilities and e-mail alert options. In the JET specific papers the diagrams contained within the PDFs on this site are hyperlinked.

Kinetic modelling of the detached divertor plasma

D. Tskhakaya*

Institute of Applied Physics, TU Wien, Fusion@ÖAW, 1040 Vienna, Austria
Institute of Theoretical Physics, University of Innsbruck, A-6020 Innsbruck, Austria
Permanent address: Andronikashvili Institute of Physics, 0177 Tbilisi, Georgia

Received XXXX, revised XXXX, accepted XXXX
Published online XXXX

Key words Edge plasma, PIC simulations, detached plasma

Implementation of self-consistent model of plasma recombination into the BIT1 PIC code and the simulation of detached SOL plasma are described. Our simulations indicate that in a strongly recombining plasma edge the sheath properties do not change qualitatively. The most affected parameter is the sheath heat transmission coefficient, which can increase by order of magnitude.

Copyright line will be provided by the publisher

1 Introduction

The detached plasma regime is one of the most promising candidates for reducing divertor heat loads in large tokamaks to the acceptable level [1]. Typically, plasma detachment is reached at sufficiently high upstream SOL densities, leading to electron cooling in front of the divertor plates and to so called “roll over” of the divertor ion flux [2]. Physics of the plasma detachment is not yet well understood and there exist number of experimental observations, which cannot be reproduced by SOL simulating large fluid codes [3-7]. One of the possible explanations is the influence of kinetic effects, which might play dominant role in the detachment [8, 9]. Existing kinetic models of the detached plasmas are too simplified: the detachment is reached by artificially applied radial electric field and/or random removing of plasma particles in the divertor region, mimicking the plasma recombination (e.g. see [10, 11]).

The aim of the present work is to perform a self-consistent kinetic modelling of the plasma detachment and to study the characteristics of the detached plasma sheath. For the simulations we use the PIC code BIT1 [12]. Plasma recycling and recombination, as well as the impurity (carbon) sputtering and transport in the SOL are included in the model. In order to avoid artificial effects originating from applying of artificial boundary conditions at the divertor plasma, we simulate the entire SOL.

The paper is organised as follows: in the next section we describe implementation of radiative and three-body (TB) recombination processes in the BIT1 code, in the Sec. 3 we present simulation results, which are discussed in the Conclusions.

2 Implementation of recombination processes

BIT1 code includes a large set of atomic, molecular and plasma-surface interaction processes, see [12] and references there. For simulation of the detached plasma we implemented two sets of recombination processes, the radiative and the TB recombinations:



where e , H^+ , $H(n)$ and H denote electrons and hydrogen isotopes in ionized, excited and ground stats, respectively; n is the principle quantum number. Atomic/molecular collisions in BIT1 code are performed via *nonlinear binary null-collision method* introduced in [13]. The collision operator consists of two steps, finding of collision pares and the collision itself (for details see [13]). Collection, derivation of the corresponding collision cross-sections represents a complex task and will be discussed in details. Below we consider the processes (1) and (2) separately.

* Corresponding author. E-mail: david.tskhakaya@tuwien.ac.at, Phone: +43 512 5076225

3.1 Radiative recombination

The collision-cross sections for radiative recombination can be derived from the *detailed balance principle* (see e.g. [14])

$$g_{H^+} p_{el}^2 \sigma_{rec}^{rad}(E, n, l) = g_H p_{phot}^2 \sigma_{ion}^{phot}(E, n, l), \quad (3)$$

where $p_{el} = \sqrt{2m_e E}$ and $p_{phot} = \mathcal{V}h/c$, $\mathcal{V}h = E + E^n = E + R_y/n^2$, are the electron and the photon momenta, E , E^n and R_y are the electron, the ionization and the Rydberg energies, n and l are the principle and the angular momentum quantum numbers, $g_{H^+} = 1$ and $g_H = 2(2l+1)$ are the statistical weights of the corresponding states, and $\sigma_{ion}^{phot}(E, n, l)$ is the photoionization collision, $H(n) + \mathcal{V}h \rightarrow e + H^+$, cross-section. After summing over angular momentum and performing simple transformations we obtain

$$\sigma_{rec}^{rad}(E, n) = \frac{n^2 \alpha^2 (E + E^n)^2}{2ER_y} \sigma_{ion}^{phot}(E, n), \quad (4)$$

where $\sigma_{ion}^{phot}(E, n)$ is the l -averaged photoionization collision cross-section described in [15, 16]

$$\sigma_{rec}^{rad}(E, 1) = \frac{2^8 \pi \alpha^3}{3} \pi a_0^2 \frac{\eta^3}{(1+\eta)^2} f(\eta), \quad f(\eta) = \frac{\exp(-4\sqrt{\eta} \arccot(\sqrt{\eta}))}{1 - \exp(-2\pi\sqrt{\eta})}, \quad \eta = \frac{R_y}{E}, \quad (5)$$

$$\sigma_{rec}^{rad}(E, n > 1) = \begin{cases} \frac{32\alpha^3 \pi a_0^2}{3\sqrt{3}} \frac{\eta^2}{n(n^2 + \eta)}, & \eta \geq \frac{n^2}{n^2 - 1} \\ \frac{8\alpha^3 \pi a_0^2}{9} \frac{\eta^{3/2}}{n^2 \sqrt{n^2 + \eta}}, & \eta < \frac{n^2}{n^2 - 1} \end{cases} \quad (6)$$

where α and a_0 are the fine structure constant and the Bohr radius. We assume that excited states of recombined atom will de-excite sufficiently fast to the ground state, so that the effective radiative recombination cross-section represents a sum of $\sigma_{rec}^{rad}(E, n)$ over the principle quantum number n . This cross-section and the corresponding rate coefficient are plotted in Figs. 1 and 2.

The collision operator for radiative collisions is relatively simple: the colliding particles, the electron and H^+ ion are removed from the simulation and a new atom is introduced. The velocity of the atom is obtained using momentum and energy conservation constrains and given as

$$\vec{V}_H = \vec{V}_{H^+} + \vec{V}_{el} m_e / M_i \approx \vec{V}_{H^+}. \quad (7)$$

3.2 Three-body recombination

We cannot find TB recombination cross-sections in the literature and derived it using the detailed balance principle. Let us assume that the corresponding collision cross-section, $\sigma_{TBR}(E_1, E_2, n)$, depends only on incoming electron energies, E_1 , E_2 , on principle quantum number of the product atom and neglect the motion of the massive target and the product (H^+ , H). The number of TB recombination events, when initial two electrons have the energies $E_1 \div E_1 + dE_1$ and $E_2 \div E_2 + dE_2$ is calculated as

$$dN_{TBR} = V_1 V_2 \sigma_{TBR}(E_1, E_2, n) n_e^2 n_{H^+} f_e(E_1) f_e(E_2) dE_1 dE_2. \quad (8)$$

Here n_{e, H^+} are the electron and the ion densities, $V_{1,2} = \sqrt{2E_{1,2}/m_e}$ and are electron velocities and electron energy distribution function (EDF). The number of ionization events when the initial and the secondary electrons have the energies $E_1' \div E_1' + dE_1'$, $E_2 \div E_2 + dE_2$, is given as

$$dN_{ion} = V_1' \sigma_i(E_1' | E_2, n) n_e n_H f_e(E_1') dE_1' dE_2, \quad (9)$$

where $V_1' = \sqrt{2E_1'/m_e}$ is the energy of the primary electron, n_H is the density of atoms and $\sigma_i(E_1' | E_2, n)$ is the doubly-differential cross-section for ionisation from the state with the given n . In the thermodynamic equilibrium we have [17]

$$dN_{TBR} = dN_{ion}, \quad f_e(E) = f_{Maxw}(E) = \frac{2}{\sqrt{\pi}} \frac{\sqrt{E}}{T^{3/2}} \exp(-E/T),$$

$$\frac{n_e n_p}{n_H} = \frac{(2\pi m_e T)^{3/2}}{h^3 n^2} \exp(-E_n/T)$$
(10)

leading to the following expression for the TB recombination cross-section:

$$\sigma_{TBR}(E_1, E_2, n) = 4R_y^{3/2} (2m_e)^{1/2} n^2 \pi^2 a_0^3 \frac{E_1 + E_2 + E^n}{E_1 E_2} \sigma_i(E_1 + E_2 + E^n | E_2, n). \quad (11)$$

Here we use the energy conservation constrain: $E_1' = E_1 + E_2 + E^n$. It has to be noted that in literature the ionization double-differential cross sections are given for a distinguishable case, i.e. the index "2" corresponds explicitly to the secondary electron with $E_2 < (E_1 - E^n)/2$, while in (11) we do not distinguish which electron was born during the ionization. Hence, for explicit calculations we consider

$$\sigma_i(E_1' | E_2, n) \rightarrow \frac{1}{2} (\sigma_i(E_1' | E_2, n) H(E_1' - E_0 - 2E_2) + \sigma_i(E_1' | E_1, n) H(2E_2 - E_1' + E_0)), \quad (12)$$

where H is the Heavside step-function. For hydrogen isotopes we use the doubly-differential cross-sections from [18], which we generalize for $n > 1$:

$$\sigma_i(E_1, E_2, n) = \frac{A n^4}{E_n \varepsilon_1} \left(\frac{1}{\varepsilon_1^2} + \frac{1}{(\varepsilon_1 - \varepsilon_2)^2} - \frac{1}{\varepsilon_1 \varepsilon_2} - \frac{1}{\varepsilon_1 (\varepsilon_1 - \varepsilon_2)} + \frac{\ln \varepsilon_1}{n \varepsilon_2^3} \sum_{i=0}^3 \frac{a_i}{\varepsilon_2^i} \right), \quad \varepsilon_{1,2} = 1 + E_{1,2} / E^n; \quad (13)$$

$$A = 0.3440, \quad a_0 = -0.014353, \quad a_1 = 0.75206, \quad a_2 = -0.29548, \quad a_3 = 0.056884.$$

In Fig. 2 are plotted rate coefficients (i.e. double Maxwell-averaged $V_1 V_2 \sigma_i(E_1, E_2, n)$) obtained from Eqs. (12), (13), showing good agreement with the existing data from [19]. In Fig. 1 are shown the ordinary differential cross sections, $\sigma_i(E_1, n) = \int \sigma_i(E_1, E_2, n) dE_2$ indicating that these cross sections are extremely sensitive to the colliding electron energies.

The TB recombination cross-section represents a strongly increasing function of n , $\sigma_{TBR}(E_1, E_2, n) \sim n^6$. As a result, the particles are recombined mainly in highly excited atom states, which are re-ionized back (the ionization rates scale as $\sim n^2$). The upper limit of $n = n_{max}$ when most of the recombined atoms are de-excited (and not re-ionized back) depends on plasma parapets. According to the simplified model from [20] $n_{max} \sim \sqrt{R_y / T_e} \sim 4$, while in complex collisional-radiative models up to $n_{max} = 20$ are considered [21]. In our simulations we consider different cases $n_{max} = 1, 8, 15$ and 20 and assume that all atoms with $n > n_{max}$ are re-ionized back, while others de-excite to the ground state. The corresponding total cross-sections and state averaged bound energies are obtained as follows:

$$\sigma_{TBR}(E_1, E_2) = \sum_{n=1}^{n_{max}} \sigma_{TBR}(E_1, E_2, n), \quad \bar{E} = \sum_{n=1}^{n_{max}} P^n E^n \approx R_y \sum_{n=1}^{n_{max}} n^4 / \sum_{n=1}^{n_{max}} n^6, \quad (14)$$

where $P^n \sim n^6$ is the relative probability of the TBR recombination to the state n .

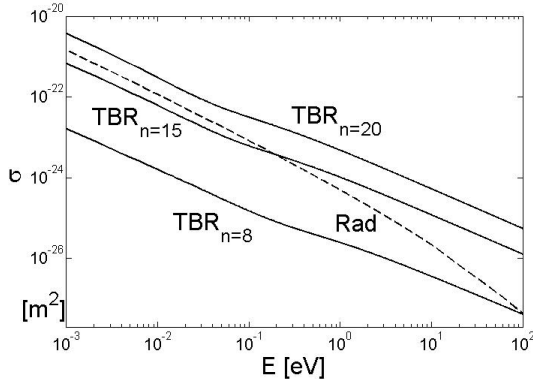


Fig. 1 Radiative (Rad) and TB (TBR) recombination cross-sections. For the TB recombination $n_e = 10^{20} \text{ m}^{-3}$ and $E_2 = 0.01 \text{ eV}$ are assumed. Radiative recombination cross section is summed over $n = 1-10^6$.

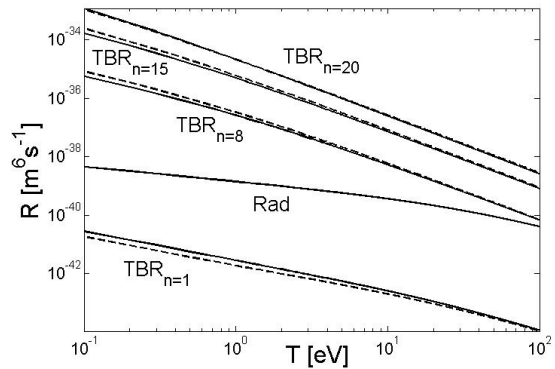


Fig. 2 Radiative and TB recombination collision rates. The radiative recombination rate is divided by $n_e = 10^{20} \text{ m}^{-3}$. TBR solid and dashed lines correspond to the rates from (12, 13) and [19], respectively.

In the simulation different triplets (two e and one H^+) are analyzed in each cell and the probability of TB recombination collision is calculated according to $P = 1 - \exp(-V_1 V_2 \sigma_{TBR}(E_1, E_2) n_e n_i \delta t)$, where δt is the simulation time step. The after-collision velocities of particles are calculated from the momentum and energy conservation equations:

$$\begin{aligned} \vec{V}'_1 &= \vec{V}_{H^+} + \vec{U}, \quad U = \sqrt{(\vec{V}_1 - \vec{V}_{H^+})^2 + (\vec{V}_2 - \vec{V}_{H^+})^2 + 2\bar{E}/m_e}, \\ \vec{V}'_H &= \vec{V}_{H^+} + (\vec{V}_1 + \vec{V}_2 - \vec{V}'_1) m_e / M_i \approx \vec{V}_{H^+}. \end{aligned} \quad (15)$$

The velocity \vec{U} is isotopically scattered.

3 PIC simulations

Fully self-consistent quantitative kinetic modelling of the detached plasma requires multidimensional treatment, as well as inclusion of different atomic and molecular processes. In the present paper we consider a qualitative model keeping simulated plasma edge as simple as possible: the model includes electrons, deuterium ions and atoms, impurity atoms and ions (C, C^+) and nonlinear interaction between them. Plasma recycling coefficients at the divertors are assumed to be 1. Impurity atoms are physically and chemically sputtered from the divertor plates and are used as a plasma (electron) cooler. In order to avoid use of artificial boundary conditions in the divertor plasma we consider the whole SOL, so that plasma conditions at the boundary develop self-consistently. For the simulation we employ the electrostatic PIC-Monte Carlo code BIT1 [22]. The simulation geometry corresponds to the magnetic flux tube in the SOL bounded between the divertor plates, separatrix and outer wall. Charged and neutral particles are treated in 1D and 2D, respectively. The details of this SOL-simulation technique can be found in [12] and references there. We consider different C sputtering coefficients, $\gamma_C = 0.01, 0.08$, and different $n_{\max} = 0, 8, 15, 20$ for TB recombination ($n_{\max} = 0$ correspond to the case without recombination). SOL size corresponds to JET, the magnetic field inclination angle to the divertor surface is 6° . In order to ensure high accuracy of simulations large number of 1D cells (3.6×10^5) and particles per cell (70 – 900) have been used. Simulations were running on HELIOS supercomputer employing 1024 cores per run.

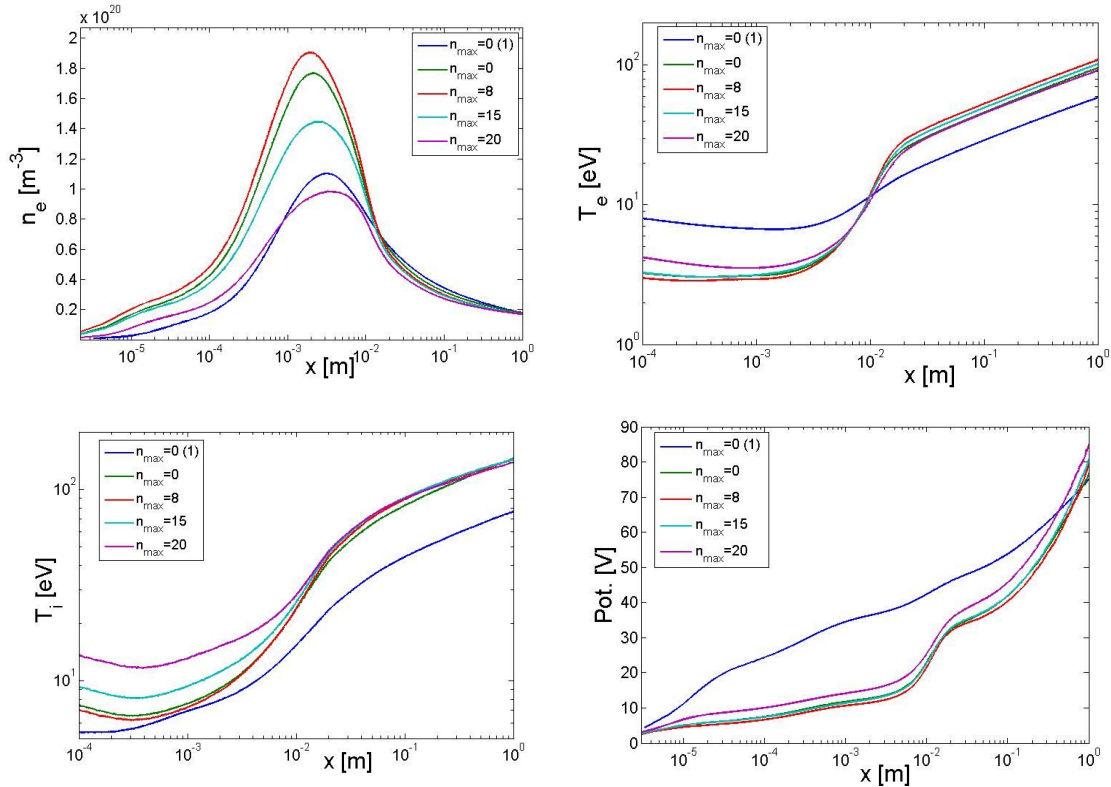


Fig. 3 Poloidal profiles of the electron density and temperature, of the D^+ temperature and the plasma potential at the inner divertor. $\gamma_C = 0.08$, except the case '(1)' when $\gamma_C = 0.01$. x denotes the distance from the divertor surface.

Poloidal profiles of the plasma density, the temperature and the potential in the divertor plasma are shown in Fig. 3. Qualitatively, plasma profiles do not change with recombination. For small recombination rate, $n_{\max}=8$, the plasma density increases, but then it decreases with increasing recombination rate. Mach number, $M = V_{\parallel, D^+} / c_s$, $c_s = \sqrt{(T_e + T_i) / M_i}$, profiles are plotted in Fig. 4. The location of the sheath entrance (i.e. the point where $M=1$) does not change significantly.

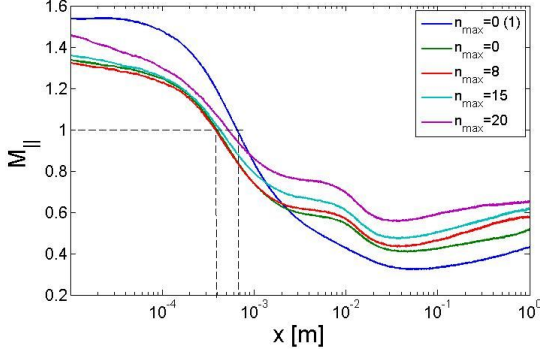


Fig. 4 Poloidal profiles of the Mach number at the inner divertor.

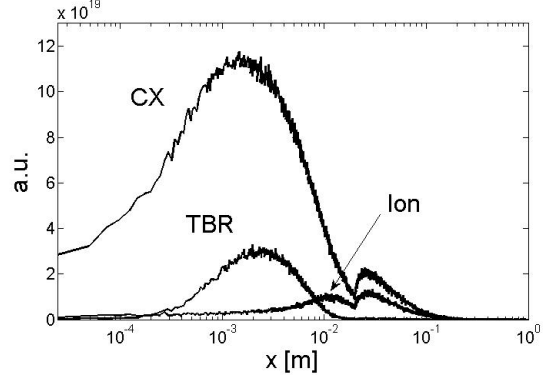


Fig. 5 Poloidal profiles of TB recombination, D ionization (Ion) and $D + D^+$ charge exchange (CX) collision events at the inner divertor. The case $n_{\max} = 20$. The radiative recombination is negligibly small.

As we see, plasma profiles do not change significantly even for a strong negative particle source (i.e. recombination). The explanation can be found from the profiles of different atomic collision events given in Fig. 5: although the recombination rate in front of the sheath exceeds the ionization one, it is still lower than the charge-exchange rate. As a result, the total friction force in D^+ momentum conservation equation stays negative $R_{\parallel} \approx -(v_{ion} + 2v_{cx} - v_{rec})V_{\parallel, D^+}$, where v_{ion} , v_{cx} and v_{rec} denote the ionization, the charge exchange and the recombination collision frequencies, respectively. This equation describes plasma sheath profiles, so that if the condition $v_{ion} + 2v_{cx} - v_{rec} > 0$ is satisfied, then these profiles do not differ qualitatively from the “classical” ones. Contrary to this, the parameters depending on high energy particle fluxes can strongly deviate from the classical values. As an example, in Figs. 6 and 7 are plotted the sheath heat transmission factor (SHTF), $q_{div} / F_{D^+} T_e$, and the normalized potential drop across the sheath; here q_{div} and F_{D^+} are power and particle (D^+) fluxes to the divertor plates.

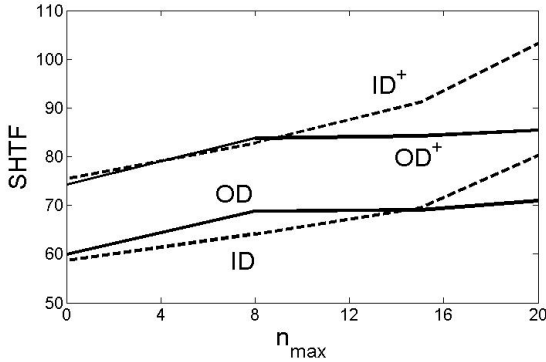


Fig. 6 Sheath heat transmission factors at the inner (ID) and outer (OD) divertors. The upper index “+” denotes total heat fluxes including D atom contribution.

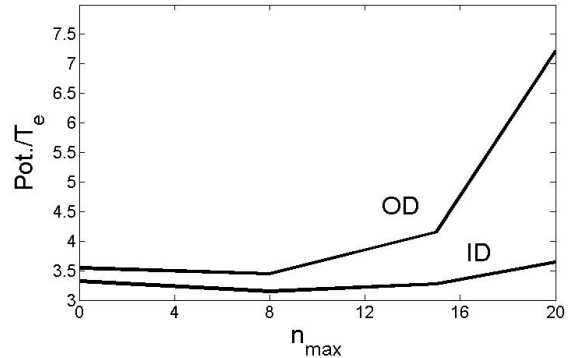


Fig. 7 Normalized potential drop across the sheath.

Increase of the SHTF and of the sheath potential drop is the consequence of high concentration of superthermal particles carrying significant fraction of total energy. Moreover, as we can see from Fig. 6, a non-negligible amount of this energy is transferred by the atoms originating from the charge exchange and the recombination collisions. As a result, the total heat load to the divertors does not change significantly with increasing recombination rate, as this happens for the particle flux (see Fig. 8).

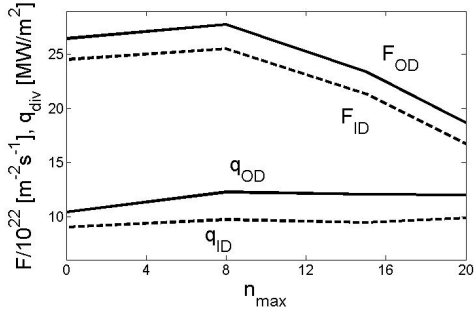


Fig. 8 Particle (D^+) and heat fluxes to the divertor plates.

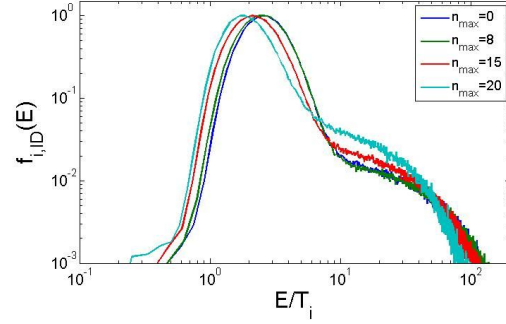


Fig. 9 Energy distribution function of the D^+ ions absorbed at the inner divertor.

4 Summary

We have derived doubly-differential cross-sections for TB recombination and implemented the corresponding TB and radiative recombination modules into the BIT1 code. Our simulations indicate that plasma recombination does not change plasma profiles at the divertors qualitatively. The explanation of this observation is the fact that the charge-exchange collisions still play the dominant role even in the strongly recombining divertor plasma. Contrary to this, number of sheath parameters, which depend on concentration of super-thermal energetic particles, might change up to the order of magnitude. The effect of such particles can be explicitly seen from the energy distribution function (EDF) of particles observed at the divertor plates (see Fig. 9). These EDFs clearly exhibit double, low and high energy, fractions. The latter represent energetic particles flying almost collisionless through the divertor plasma. Contribution of these particles, as well as atoms originating from charge-exchange and recombination collisions, cannot be neglected in estimation of heat loads to the divertor plates.

Acknowledgements. This work has been carried out within the framework of the EUROfusion Consortium and has received funding from the Euratom research and training program 2014–2018 under grant agreement No 633053. The views and opinions expressed herein do not necessarily reflect those of the European Commission. The author acknowledges the support by the project FWF P26544-N27 and useful discussions with M. O'Mullane. Numerical simulations have been carried out using the HELIOS supercomputer system at Computational Simulation Centre of International Fusion Energy Research Centre (IFERC-CSC), Aomori, Japan, under the Broader Approach collaboration between Euratom and Japan, implemented by Fusion for Energy and JAEA.

References

- [1] M. Wischmeier, et al., *J. Nucl. Mater.*, **463**, 22 (2015).
- [2] P. C. Stangeby, *The Plasma Boundary of Magnetic Fusion Devices* (IOP, Bristol and Philadelphia, 2000).
- [3] M. Groth, A.M. Mahdavi, G.D. Porter and T.D. Rognlien, *Contr. Plasma Phys.*, **42** (2-4), 389 (2002).
- [4] M. Wischmeier, M. Groth, A. Kallenbach, et al., *J. Nucl. Mater.*, **390–391**, 250 (2009).
- [5] Kotov, D. Reiter, D.P. Coster and A.S. Kukushkin, *Contr. Plasma Phys.*, **50** (3-5), 292 (2010).
- [6] K. Hoshino, K. Shimizu, T. Takizuka, et al., *Plasma Fusion Res. SERIES*, **9**, 592 (2010).
- [7] S. Wiesen, W. Fundamenski, M. Wischmeier, et al., *J. Nucl. Mater.*, **415**, S535 (2011).
- [8] D. Coster, *J. Nucl. Mater.*, **415**, S545 (2011).
- [9] S. Potzel, M. Wischmeier, M. Bernert, et al., *J. Nucl. Mater.*, **438**, S285 (2013).
- [10] T. Takizuka and M. Hosokawa, *Contr. Plasma Phys.*, **40** (3-4), 471 (2000).
- [11] T. Takizuka, M. Hosokawa, K. Shimizu, *J. Nucl. Mater.*, **290–293**, 753 (2001).
- [12] D. Tskhakaya, M. Groth and JET contributors, *J. Nucl. Mat.*, **463**, 624 (2015).
- [13] D. Tskhakaya, S. Kuhn, Y. Tomita, et al., *Contrib. Plasma Phys.*, **48** (1-3), 121 (2008).
- [14] E. Bauer, *Phys. Rev.*, **84** 2, 315 (1951).
- [15] H. Bethe and E. Salpeter, *Quantum Mechanics of One- and Two-Electron Atom Systems* (Ac. Press, New York, 1957).
- [16] I.I. Sobelman, *Atomic Spectra and Radiative Transitions* (Springer-Verlag, Berlin-Heidelberg, 1981).
- [17] M. Saha, *Philosophical Magazine Series 6*, **40** (238), S. 472 (1920).
- [18] Yong-Ki Kim and M. Eugene Rudd, *Phys. Rev. A*, **50** (5), 3954 (1994).
- [19] R.K. Janev, D. Reiter, U. Samm, *Collisional and Radiative Processes in Hydrogen Plasmas*, (IPP Report 4105, 2003).
- [20] E. Hinno and J. Hirschberg, *Phys. Rev.*, **125** (3), 795 (1962).
- [21] M. O'Mullane, private discussions.
- [22] D. Tskhakaya, A. Sobba, et. al., *Proceedings of 18-th Euromicro Conference, Pisa Italy, IEEE*, 476 (2010).